Biogeosciences Discuss., 6, 6839–6887, 2009
www.biogeosciences-discuss.net/6/6839/2009/

Biogeosciences Discussions

Biogeosciences Discussions is the access reviewed discussion forum of *Biogeosciences*

Ultraphytoplankton distribution and upper ocean dynamics in the eastern Mediterranean during winter

M. Denis[1], **M. Thyssen**[1], **V. Martin**[1], **B. Manca**[2], **and F. Vidussi**[3,*]

[1]Laboratoire de Microbiologie, Géochimie et Ecologie Marines, Université de la Méditerranée, CNRS UMR 6117, 163 avenue de Luminy, Case 901, 13288 Marseille cedex 9, France
[2]Istituto Nazionale di Oceanografia e Geofisica Sperimentale – OGS, Borgo Grotta Gigante, 42/c, 34010 Sgonico (Trieste), Italy
[3]Laboratoire d'Océanographie de Villefranche, CNRS UMR 7093, Université de Paris VI, quai de la Darse, B.P. 28, 06234 Villefranche-sur-mer cedex, France
[*]present address: Ecosystèmes lagunaires, CNRS, UMR 5119, Université Montpellier II, CP 093, Place Bataillon, 34095 Montpellier cedex 5, France

Received: 12 May 2009 – Accepted: 6 June 2009 – Published: 13 July 2009

Correspondence to: M. Denis (michel.denis@univmed.fr)

Published by Copernicus Publications on behalf of the European Geosciences Union.

Abstract

The vertical distribution of ultraphytoplankton (<10 μm) was determined in the upper 200 m of the eastern Mediterranean during the winter season. Four clusters were resolved by flow cytometry on the basis of their optical properties and identified as *Synechococcus*, *Prochlorococcus*, pico- (<3 μm) and nanoeukaryotes (3–10 μm). *Synechococcus* was the most abundant population (maximum abundance of about 37 000 cells cm^{-3}) and contributed up to 67.7% to the overall ultraphytoplanktonic carbon biomass, whereas the contribution of *Prochlorococcus* never exceeded 6.5%. The maximum integrated carbon biomass was 1763, 453, 58 and 571 mg C m^{-2} for nanoeukaryotes, picoeukaryotes, *Prochlorococcus* and *Synechococcus*, respectively. Water mass properties were analyzed on the basis of temperature and salinity distributions in order to account for the general circulation and locate the main hydrodynamic structures (fronts, gyres, transition between western and eastern basins). Relationships were established between the ultraphytoplankton distribution and the hydrological characteristics of the main hydrodynamic structures. Significant relationships were found between *Synechococcus* abundance and density, resulting from the impact of a gyre in southern Adriatic and a thermohaline front in the Ionian Sea. A significant relationship was also found between picoeukaryotes and salinity in the comparison of western and eastern Mediterranean. Relationships were only significant for the most abundant clusters. As the first investigation of ultraphytoplankton winter distribution in the eastern Mediterranean, the present study will significantly contribute to a better knowledge of the ultraphytoplankton structure over seasons and of its dependence on hydrological features.

1 Introduction

Hydrodynamism in the oceans is known to control phytoplankton distribution. In particular, meso-scale hydrodynamic structures such as fronts, eddies and gyres control

BGD

6, 6839–6887, 2009

the biomass and primary production (McGillicuddy et al., 1998) as well as phytoplankton composition (e.g. Rodriguez et al., 2001; Vidussi et al., 2001). Hydrodynamic structures and circulation can influence directly via vertical motion the phytoplankton size structure (Rodriguez et al., 2001). At the same time hydrodynamic structures drive nutrients or modify the light environment and thus indirectly control phytoplankton biomass and composition (Vidussi et al., 2001). The Mediterranean is an ideal region to study physical-biological relationships as different hydrodynamic structures (mesoscale of 10–100 km) occur at relative small scales which can be simultaneously sampled for physical and biological parameters (Claustre et al., 1994; Rodriguez et al., 2001; Vidussi et al., 2001).

The general Mediterranean circulation is characterized by an inflow of Atlantic Water (AW) at surface and a non return westward deeper flow of the dominant water mass of the Mediterranean, the Levantine Intermediate Water (LIW), into the Atlantic Ocean (Wüst, 1961). As a consequence the Mediterranean is potentially oligotrophic because of the inflow of generally nutrient poor Atlantic surface waters. However, the LIW is known to play an important role in transporting inorganic nutrients around the basin and further on in the Atlantic Ocean (Béthoux, 1979). In fact the LIW affects wintertime dense water formation processes both in the eastern and western basin (Schlitzer et al., 1991; Leaman and Schott, 1991), creating conditions of vertical transfer of nutrient-rich intermediate/deep waters close to the surface for the biological consumption. This is the case for example of the north western Mediterranean where deep convection occurs during winter followed by spring phytoplancton bloom and further by oligotrophy in summer (Marty et al., 2002). At the same time, in the eastern Mediterranean the thermohaline circulation and physical processes establish conditions of low nutrient content and low primary production (Azov, 1986, Psara et al., 2000; Tselepides et al., 2000). Thus the Mediterranean is considered as ultra-oligotrophic or mesotrophic, depending on the studied area and the season (Berman et al., 1984; Minas et al., 1988; Conan et al., 1998, Krom et al., 2003, 2005). However, among the different Mediterranean regions, the eastern Mediterranean is by far the most oligotrophic re-

gion. The general circulation of the eastern Mediterranean has been intensively investigated by the POEM group (1992), which provided evidence of different scales, dynamics and variabilities. Four main regions may be distinguished, i.e. the Adriatic, the Ionian, the Aegean and the Levantine basins, which exhibit different hydrodynamic regimes and processes that have been revealed important for biological and chemical dynamics. Superimposed to the basin-wide thermohaline cell circulation at surface, permanent and/or recurrent sub-basin scale gyres exist: the permanent cyclonic gyre south-west of Crete, the recurrent Ierapetra anticyclone south-east of Crete, the permanent cyclonic gyre near Rhodes connected to the western Cyprus Cyclonic gyre in the northern Levantine, and finally, the complex of the multi-lobe Mersa-Matruh and the transient Shikmona anticyclones dominates the Levantine basin in the south. These gyres isolate water masses and therefore, they have a large impact on phytoplankton development, such as stimulating it by upward inflows of nutrients.

In the eastern Mediterranean, nutrient content and primary production can be very low (Azov, 1986), as in the Cretan basin (Psara et al., 2000; Tselepides et al., 2000), thus several extremely nutrient-poor areas of the eastern Mediterraean are ultra-oligotrophic (Krom et al., 2003, 2005; Thingstad et al., 2005). In addition, phosphorus limitation of phytoplankton and bacteria growth was suggested by Berland et al. (1980) and this was confirmed by several studies (Krom et al., 1991; Vaulot et al., 1996; Zohary and Robarts 1998; van Wambeke et al., 2002; see also a review in Krom et al., 2003). In addition, a recent lagrangian in situ P-addition experiment carried out in an ultra-oligotrophic region of the eastern Mediterranean (Krom et al., 2005) showed that bacteria was conventionally P-limited and phytoplankton was N and P-co limited (Thingstad et al., 2005; Zohary et al., 2005). In oligotrophic waters, a number of studies have shown that ultraphytoplankton (<10 μm) makes the most abundant fraction of phytoplankton and that it plays a major role in the overall primary production (Li et al., 1993; Platt et al., 1983; Yacobi et al., 1995; Vidussi et al., 2001; Psarra et al., 2005). For instance, over 85% of chlrophyll a in the eastern Basin belong to the <10 μm size fraction (Li et al., 1993). This autotrophic ultraphytoplankton is mainly

composed of cyanobacteria, with dominance of *Synechococcus* over *Prochlorococcus* (Waterbury et al., 1986; Martin, 1997; Denis et al., 2000; Casotti et al., 2003; Psarra et al., 2005) and of eukaryotes belonging to the group of chlorophyceae, prasinophyceae and prymnesiophyceae (Vidussi et al., 2001; Psarra et al., 2005). Some unicellular cyanobacteria are thought to fix dissolved dinitrogen (Zehr et al., 2001), enabling them to grow despite the very low nutrient content (Bonin et al., 1989). However, the importance of dinitrogen fixation in the Mediterranean remains still unknown (Psarra et al., 2005; Thingstad et al., 2005).

In this oligotrophic region the hydrodynamic structures may induce nutrient enrichments and stimulate biological activity with respect to surrounding areas. Consequently, they may play a significant role in the development of phytoplankton and largely affect the distribution and structure of ultraphytoplankton in the eastern Mediterranean (Casotti et al., 2003). The phytoplankton distribution in the eastern Mediterranean is poorly documented and very fragmented (Li et al., 1993; Yacobi et al., 1995; Magazzu and Decembrini 1995; Psarra et al., 2005). These studies showed that the Levantine Basin was dominated by cyanobacteria, mainly *Synechococcus*. In contrast, eukaryote ultraphytoplankton was found in smaller numbers.

In the present study we report the first vertical distribution of ultraphytoplanktonic cells ($<10\,\mu$m) determined by flow cytometry over most of the eastern Mediterranean during winter (January 1995). Results are discussed with respect to some hydrological structures with which relationships could be established. In addition, comparisons are made with few vertical distributions observed in the western Mediterranean during the same period.

2 Materials and methods

2.1 Study area and sampling

Data were collected during the basin-wide R/V METEOR cruise M31/1 (30 December 1994 to 5 February 1995), conducted in the frame of the POEM/BC (Physical Oceanography of the eastern Mediterranean – Biology, Chemistry) and the EU/MAST-MTP (Marine Science and Technology-Mediterranean Targeted Project) of the European Union programme.

The hydrographic work was conducted over a series of 77 full-depth hydrological stations (Fig. 1), while the vertical distribution of ultraphytoplankton in the upper 200 m was determined at selected 47 stations, 4 in the western and 43 in the eastern Mediterranean, (Fig. 1), lowering a SeaBird-911 Plus conductivity-temperature-depth profiler (CTD), equipped with a Sea Teach fluorometer, an oxygen sensor and a rosette water sampler of 24 Niskin bottles of 10 l. The seawater samples were collected during the up-cast at selected depths between 0 to 200 m, according to the most important features displayed by the fluorometer profiles during the down-cast. Four vertical profiles were analyzed in the western Mediterranean for the sake of comparison.

2.2 Hydrography

The temperature and salinity data were continuously checked against independent measurements to a precision of ±0.002 performed by digital reversing thermometers and water sample analyses on board using an AUTOSAL Guildline bench salinometer. The overall discrepancies were typically less than ±0.005 units. Through the text, the temperature is given as potential temperature (θ), the salinity is according to the practical salinity scale and the density is reported as potential density excess (σ_θ).

The horizontal maps of the hydrographic fields were constructed by extracting temperature, salinity and density values in the upper 10 m and averaging them on the vertical. The data were objectively analysed on a regular grid of 1/4° using an isotropic

BGD
6, 6839–6887, 2009

correlation function (Carter and Robinson, 1987) after detrending by a first order polynomial function. The derived fields are not represented in the maps where the errors exceeded 60%.

The mixed layer depth (MLD), mostly represented by a homogeneous distribution of the temperature, salinity and density fields, results from a turbulent mixing due to atmospheric forcing and undergoes substantial temporal variations ranging from diurnal to seasonal and longer time scales. The choice of appropriate criteria in the definition of the MLD may have strong influence on studies of heat and salinity budgets as well as on biological and chemical processes (de Boyer Montégut et al., 2004, and references therein). In the Mediterranean Sea the salinity is a relevant parameter in determining the MLD, particularly in wintertime when the Atlantic Water plays the fundamental role in establishing the density gradients. Therefore, the density represents a good parameter in estimating the vertically homogeneous mixed layer. Moreover, since we want to estimate the depth through which the water column has been mixed over a time scale longer than the diurnal variability, practical reasons have suggested to exclude the layer close to the surface avoiding the so called "skin effect".

In this context, we have used the threshold method and the MLD is the depth at which the potential density (σ_θ) varies by a given threshold value ($\Delta\sigma_\theta$) from that at a near-surface reference depth (Z_{ref}). After a visual inspection of the CTD profiles in the different regions analyzed, the Z_{ref} is set at 2 m to avoid a large part of density gradient due to the diurnal variability and a $\Delta\sigma_\theta$ of 0.02 kg m^{-3} seems a good compromise. The MLD calculated with a threshold value of $\Delta\sigma_\theta$=0.05 kg m^{-3} often falls within the seasonal thermocline rather than at its top. However in some stations the mixed layer is characterised by a shallower actively mixing layer and an underlying layer that have been mixed within last few weeks or months. In these circumstances the threshold value of 0.05 kg m^{-3} has been chosen.

2.3 Flow cytometry

The seawater samples were collected at 12 different depths between 0 and 200 m, fired during the up-cast at selected depths according to the most important features displayed by the fluorometer profiles during the down-cast. For flow cytometric analysis, seawater samples (100 to 150 cm^3) from Niskin bottles were prefiltred on 100 μm mesh size net to prevent clogging of the flow cell and homogenized. Subsamples of 5 ml were fixed with 2% paraformaldehyde and stored in liquid nitrogen up to analysis in the laboratory (Trousselier et al., 1995; see also Vaulot et al., 1989).

Single cell analysis was run with a CYTORON ABSOLUTE (ORTHO Diagnostic Systems) flow cytometer, equipped with an air-cooled argon laser (excitation wavelength at 488 nm). Each cell was characterized by 5 optical parameters: two scatter parameters, namely forward angle scatter (related to the particle size) and right angle scatter (related to cell structure and shape), and three fluorescence parameters related to emissions in the red (>620 nm), orange (565–592 nm) and green (515–530 nm) wavelength ranges. Data were collected and stored in list-mode on a personal computer with the IMMUNOCOUNT software (ORTHO Diagnostic Systems). Due to the control of the sample volume by a micro-syringe, this software can directly provide cell concentrations (cells mm^{-3}). The Winlist software (Verity Software, USA) was used to determine statistical data.

Just before analysis, samples were rapidly thawed in a 30°C water bath and fluorescent beads of 10 μm in diameter were added in order to normalize the flow cytometer settings and to provide a reference for concentration calculations.

The cell concentration of each cluster was integrated at each station between 0 to 200 m depth with the trapezoid method. Interpolation of integrated cell concentration and cartography were realized with the ODV software (Schlitzer, 2003) over the domain occupied by sampled stations.

BGD
6, 6839–6887, 2009

2.4 Biomass estimation

Synechococcus abundances were converted in carbon biomasses by using the estimation of 200 fg C cell^{-1} (Mackey et al., 2002). The content of 49 fg C cell^{-1} was applied to *Prochlorococcus* (Caillau et al., 1996). For small and large eukaryotes, we used averaged biovolumes estimated by flow cytometry (4.48 and 113.10 μm^3, respectively) and the equation of Verity et al. (1992):

$$C(pg) = coeff * biovolume(\mu m^3)^{0.866} \quad (1)$$

with coeff values of 0.405 and 0.239 for small and large eukaryotes respectively. These values were derived from the curve constructed by using the set of coeff-cell size in Verity et al. (1992).

The resulting carbon biomasses per cell are 1.393 and 14.133 pg C cell^{-1} for small and large eukaryotes, respectively.

2.5 Pigment analysis

Pigments (chlorophylls and carotenoïds) were collected at the same stations and depths as samples for flow cytometric analysis. Pigments were analyzed by HPLC with the method of Vidussi et al. (1996) as detailed in Vidussi et al. (2001). Total chlorophyll a (total Chl *a*) was calculated as the sum of chlorophyll *a* and divinyl-chlorophyll *a*. The total Chl *a* concentrations determined by HPLC during this cruise were integrated over the 0–200 m layer and converted in terms of carbon by using the conversion factor C/Chl *a*=50 (Brown et al., 1999), assuming a constant ratio in the study area.

BGD
6, 6839–6887, 2009

3 Results

3.1 Water mass properties and their horizontal and vertical distributions in the upper ocean

3.1.1 The water masses of the eastern Mediterranean

The water mass properties and their transformation throughout the eastern Mediterranean were analyzed by potential temperature/salinity diagrams constructed separately for three regions: (i) the Ionian basin, (ii) the Cretan Passage, and (iii) the Levantine basin. These diagrams are depicted in Fig. 2. Low salinity values indicate the AW that intruded into the Ionian basin through the Strait of Sicily, where it was characterized by S≅37.5–38.0 and θ≅15–16°C (not shown). In the Ionian basin (Fig. 2a), the AW had salinity and temperature values in the range from 38.1 to 38.4 and from 15°C to 17°C, respectively. As it moves eastward, it might be still recognized by low-salinities; in the Cretan Passage (Fig. 2b), relatively fresh waters were found at the southernmost stations, i.e. at stations 30, 49 and 50, with salinity in the range of 38.4 to 38.8 and above the isopycnal surface 28.8 kg m^{-3}. This is a clear manifestation of the eastward flow pattern of the AW into the Levantine basin (Fig. 2c), where it may be still recognised by temperature of about 17°C and salinity in the range of 38.5–38.9, above the isopycnal 28.6 kg m^{-3}. In the Levantine basin, higher salinities (S>39.0) at surface indicate Levantine Surface Water (LSW), which results from the excess evaporation over precipitation and from the absence of fresh water from riverine inputs in this region. The LSW flowed westward through the Cretan Passage, where its salinity and temperature values ranged from 38.9 to 39.1 and 16.0°C to 17.0°C, respectively. The isopycnal 28.8 kg m^{-3} separates the upper mixed layer from the layer below.

A strong halocline appears between the isopycnal surfaces 28.8 and 29.0 kg m^{-3}, in particular in the Ionian basin, indicating the transition from the AW to the LIW, which is at deeper level, i.e. between 200 and 800 m. The LIW appears in the diagrams as a spur with salinities in the range of 39.2 to 38.8 and temperatures of 16.5°C to 14.5°C

BGD
6, 6839–6887, 2009

as it moves from the Levantine basin to the western Ionian.

In the deep layer, i.e. below the 29.17 kg m^{-3}, located at about 1000 m, water mass properties indicated a slow and steady decrease of the temperature and salinity towards the bottom, ascribed primarily to the presence of the EMDW of Adriatic origin; the abrupt changes in temperature and salinity in the very deep layer (σ_θ>29.2 kg m^{-3}) is due to the presence of the CDW recently overflowed throughout the Cretan Arc Straits into the central region all around the Crete island (Roether et al., 1996).

3.1.2 Horizontal analyses

The horizontal maps at surface were constructed for the temperature, salinity and density fields in order to illustrate the spatial distribution of the AW, LSW and their dynamics, as well. In spite of the large seasonal variability of the upper dynamics indicated by the model simulations (Roussenov et al., 1995), which have shown a prevalent eastward flow pattern of AW in winter, in January 1995 the salinity pattern reveals instead that both the western and northern Ionian were under the influence of the low-salinity AW (Fig. 3b). The upper dynamics in the Ionian basin is therefore dominated by a meandering current transporting anticyclonically AW into the northern Ionian and a strong meridional salinity front that separates AW on the west and LSW on the east (Fig. 3b). In addition, a sub-surface cyclonic eddy was centred at station 25, offshore the Greek mainland (Fig. 3c; σ_θ>28.8 kg m^{-3}). Cross tracks of temperature and salinity along the vertical have shown that this eddy was colder and saltier suggesting entrainment of highly saline water from the layer below.

In the Levantine basin, the excess evaporation over precipitation leaded to a large presence of the highly saline LSW, which dominated in the northern part of the Levantine basin and in the Aegean basin (Fig. 3b). The principal vein of the AW might be noticed in the south of the Cretan Passage and, getting progressively narrow, definitively entered into the Levantine basin along the African coast. Contrarily to previous situations depicted by Malanotte-Rizzoli et al. (1999) in 1991, when the AW was advected into the Levantine basin between the southern rim of the Rhodes gyre and the

BGD
6, 6839–6887, 2009

northern boundary of the complex Mersa-Matruh/Shikmona anticyclones, in January 1995 the AW was presumably "coastally trapped" in a very narrow band along the African coast. However, the AW has been traced as far as in the eastern Levantine basin and entrapped in the anticyclonic Shikmona gyre (Fig. 3b). In spite of the winter season, the surface temperatures were characterized by relative high values (≅17°C) throughout the southernmost portion of the eastern Mediterranean, that, in combination with low salinities (S<38.80), created conditions of low density. On the other hand, lower temperatures and higher densities dominated in the northern region enhancing winter-time convection activities and mixing in those regions prone to intermediate and deep water formation. These features may be clearly seen in the horizontal distribution of temperature, salinity and density fields (Fig. 3a–c, respectively) in the centre of the Rhodes gyre, in the south Aegean basin (Cretan basin) and in the southern Adriatic. The coherent westward flow of the LSW from the Levantine basin into the western regions occurred through the northern side of the Cretan Passage and through the Straits of the Cretan Arc. From there the LSW could be found as far as in the eastern Ionian basin.

In the southern Adriatic, upon specific hydrographic conditions associated with winter outbreaks of cold and dry continental air from the eastern Europe, just as in other sites of the Mediterranean, convective mixing and water column overturning are able to generate dense waters in the centre of the permanent and topographically controlled cyclonic gyre (Ovchinnikov, 1985). One of the most important prerequisite is the presence of the LIW, which lowers the density gradient in the sub-surface layer, allowing the exposure at surface of higher density water in the interior of the gyre. In January 1995, the winter cooling and subsequent deep convection set the properties of the water masses into the gyre towards rather low temperatures and high densities (Fig. 3a and c).

BGD
6, 6839–6887, 2009

3.1.3 Zonal section throughout the eastern Mediterranean

The spatial structure of the hydrographic fields in the upper layer is depicted in the vertical distributions of temperature, salinity, density and dissolved oxygen down to 800 m and along the transect throughout the eastern Mediterranean (Fig. 4). In particular, the transect crosses the middle Ionian, the northern side of the Cretan Passage and the convection region in the northern Levantine basin. The vertical extent of the AW within the Ionian appeared by the low salinity values down to about 200 m. Moreover, the AW exhibits dissolved oxygen values higher than those in the underlying water, which is characterized by high salinity and low oxygen contents, indicating the LIW (Fig. 4c and d).

The behaviour of isotherms, isohalines and isopycnals in the Ionian Sea indicates the presence of a bowl corresponding to the broad Ionian Anticyclone (Malanotte-Rizzoli et al., 1999), which develops down to 800 m entraining AW at surface and LIW in its interior. Thus, a frontal system was established at the surface between the relatively fresh AW on the left and the highly saline Levantine type waters on the right (Fig. 4c). In contrast, the isopycnals slope upwards from the west to the east and the doming structures prevail in the Cretan Passage and in Levantine basin. Two very strong divergence zones might be noticed. The first one was located in the Cretan Passage between the stations 32 and 46 and the second one was located in the Levantine basin (station 64). The former corresponds to the Cretan cyclone and is marked by the outcropping of the isotherm 15°C and the isopycnal 29.0 kg m^{-3} (Fig. 4a and b). The latter, much more intense, marks the Rhodes gyre where the isotherm 14.5°C and the isopycnal 29.12 kg m^{-3} were ventilating, being in direct contact with the atmosphere at the station 64. The LIW convectively formed on the periphery of the Rhodes gyre (LIWEX Group, 2003) may be recognized from the higher values of salinity and dissolved oxygen (Fig. 4c and d).

3.1.4 Mixed layer depth

MLD was computed for selected stations as shown in Table 1. Through the Sicily Straits the MLD maxima with values around 100 were found in the western and eastern straits, while in the middle it was closer to 70 m. In the eastern Ionian the MLD was >100 m in those regions dominated by the anticyclonic motion (stations 28–29) that entrains in its interior Atlantic Water. The front region is easily identified by the existing horizontal gradients in temperature and salinity towards the north-east that yields a much shallower MLD (~65 m). The mixed layer exhibited the strongest vertical uniformity in the south Adriatic reaching a depth of 463 m at station 17, where within an isolated chimney the convective overturning involved low temperature (~13°C) and highly saline water masses (S ~38.7).

3.2 Ultraphytoplankton distribution

Ultraphytoplanktonic cells (<10 μm) analyzed by flow cytometry were resolved in four clusters on the basis of their optical properties, namely nanoeukaryotes (3–10 μm), picoeukaryotes (<3 μm), *Prochlorococcus* and *Synechococcus*. The vertical distribution in the upper 200 m of each group varied independently according to depth and location. Figure 5 represents the geographic distribution of 0–200 m integrated abundances of nanoeukaryotes, picoeukaryotes, *Prochlorococcus*, and *Synechococcus* in the eastern Mediterranean and in four stations in the western Mediterranean. Integrated nanoeukaryote abundances were in the range 1.4–12.5×10^{10} cells m^{-2}. Nanoeukaryotes were poorly represented in the Ionian Sea (stations 7 to 30) (1.4 to 3.7×10^{10} cells m^{-2}) whereas nanoeukaryote integrated abundances were about twice as high (up to 6.6×10^{10} cells m^{-2}) in the Sicily Strait (station 5), in the Strait of Otranto (station 15) and in the southern Adriatic (stations 16–19). In contrast, at station 17 in the centre of the gyre in the south Adriatic, this group was poorly represented (3.4×10^{10} cells m^{-2}). In the Levantine basin, the nanoeukaryote integrated abundances were higher than in the Ionian Sea (>6×10^{10} cells m^{-2}), particularly between Cyprus and Crete islands

BGD
6, 6839–6887, 2009

(8.3 to 12.5×10^{10} cells m^{-2}) and in the Rhodes gyre where the integrated concentration values were the highest of all the eastern Mediterranean (station 57, 12.5×10^{10} cells m^{-2}). The estimated nanoeukaryote integrated carbon biomass in the upper 200 m varied between 202 and 1760 mg C m^{-2} (Table 2) following the pattern defined by their integrated abundance.

At most stations, integrated concentration values for picoeukaryotes were higher than those for nanoeukaryotes (between 5 to 35×10^{10} cells m^{-2}), but their distribution over the eastern Mediterranean followed the same pattern (Fig. 5). The Ionian basin was characterized by low values (5×10^{10} cells m^{-2}), whereas higher values were found in the Adriatic (11.5 to 19.2×10^{10} cells m^{-2}). In the Levantine basin, the integrated abundances of picoeukaryotes were similar to those detected in the Ionian basin, except at stations 31 to 36 and 40 located west of Crete, and in the Rhodes gyre (stations 51 to 71). In these two zones, the integrated concentrations were the highest over the whole eastern Mediterranean basin (15.3 to 34.9×10^{10} cells m^{-2}, Fig. 5). The estimated picoeukaryote integrated biomass in the upper 200 m varied between 18.2 and 453.3 mg C m^{-2} (Table 2) following the pattern defined by their integrated abundance.

Integrated *Prochlorococcus* abundances were between 18.5×10^{10} and 117.6×10^{10} cells m^{-2} (Fig. 5). They were low and homogeneous at the level of the Ionian sea, in the centre of the southern Adriatic gyre (station 17) and in the western side of the Levantine basin (station 54; 39.8×10^{10} cells m^{-2}). In contrast, the integrated concentration of *Prochlorococcus* were higher near the Greek coast at stations 24 and 25 (117.6×10^{10} cells m^{-2}), at station 15 and at station 16 (~80×10^{10} cells m^{-2}) located in the Otranto Strait and in the southern Adriatic, respectively; the latter station was at the periphery of the gyre, i.e. along the pattern followed by the Ionian Surface water that intruded into the Adriatic through the Strait of Otranto. In the Levantine basin, integrated abundances were relatively high (stations 55 to 74, up to 60.8×10^{10} cells m^{-2}) except in the Rhodes gyre where they were about two fold lower (~30×10^{10} cells m^{-2}, station 61). *Prochlorococcus* integrated abundances at stations sampled in the western Mediterranean were at the same levels as in the Ionian Sea (14.1×10^{10} to

24.7×10^{10} cells m^{-2}).

In the eastern Mediterranean, the integrated biomass of *Prochlorococcus* was between 9.1 to 57.6 mg C m^{-2} (Table 2) and followed the same distribution pattern as integrated concentrations. Thus, the highest *Prochlorococcus* biomasses were observed in the Ionian basin (up to 57.6 mg C m^{-2}, station 24). Integrated *Prochlorococcus* biomasses values were also relatively high in the Levantine basin (20 to 30 mg C m^{-2}).

Synechococcus was the most abundant (in terms of cell numbers) population (Fig. 5), constituting from 17% (station 5) to 68 % (station 30) of the overall ultraphytoplankton community integrated abundances. The *Synechococcus* integrated abundances ranged between 37.4 and 285.6×10^{10} cells m^{-2} (Fig. 5). In the southern Adriatic, at the periphery of the gyre (stations 19 and 16) and at the Otranto Strait (station 15), the water masses were from 4 to 5 times richer in *Synechococcus* than those at the centre of the gyre (station 17). *Synechococcus* integrated abundances were low in the western Ionian ($<120\times10^{10}$ cells m−2; stations 5 to 9) and increasing progressively towards the centre of the eastern Mediterranean. However, these values were not homogeneously distributed: for example, integrated abundances varied by an order of magnitude from 37.4×10^{10} cells m^{-2} (station 41; Aegean basin) to 285.6×10^{10} cells m^{-2} (station 47; eastern Cretan Passage). High abundances in *Synechococcus* were observed in the area occupied by the Ierapetra anticyclone located south of Crete (stations 47, 51, 54; mean concentration: 275×10^{10} cells m^{-2}); indeed, the highest value mentioned above (285.6×10^{10} cells m^{-2}) was found within this gyre. In the Rhodes gyre (stations 51–71), the *Synechococcus* integrated abundances were relatively low except at station 71 (226.0×10^{10} cells m^{-2}). In the western Mediterranean, the 4 sampled stations (2–5) were relatively poor in *Synechococcus*, with integrated abundances in the range 26.2 to 45.4×10^{10} cells m^{-2}. It is worthy to remark that these values are close to the three lowest values (33.8, 37.4 and 41.9×10^{10} cells m^{-2}) observed in the eastern Mediterranean, but in the convective regions; i.e. at stations 17, 41 and 58 located in the southern Adriatic, in the Aegean basin and in the Rhodes gyre,, respectively. *Synechococcus* was largely dominant over *Prochlorococcus*, thus

the cyanobacteria specific pigment zeaxanthin quantified by HPLC was exclusively assigned to *Synechococcus* during this study and the cell content in zeaxanthin was found depth-independent (not shown).

As a common feature, the four resolved clusters did not exhibit fluorescence increase with depth (data not shown).

In the eastern Mediterranean, the integrated (0-200 m) *Synechococcus* biomass was comprised between 67.7 and 571.2 mg C m^{-2} (Table 2). The highest values were observed in the anticyclonic Ierapetra gyre (stations 47, 51 and 54; between 540.5 and 571.2 mg C m^{-2}). Low values were found in the Sicily Strait, in the western part of the Ionian basin and in the Aegean basin (<140 mg C m^{-2}). The lowest values were found at the centre of the southern Adriatic gyre (station 17, 67.7 mg C m^{-2}). At the other stations in the eastern Ionian and in the Levantine basins, the integrated *Synechococcus* biomass was comprised between 150 and 452 mg C m^{-2}.

The carbon biomass derived from integrated Chl a concentrations analyzed by HPLC using a constant carbon/chl a ratio of 50 varied between 541 to 2549 mg C m^{-2}, with a mean value of 1122 mg C m^{-2}. The contribution percentage of *Synechococcus* and *Prochlorococcus* to this biomass was estimated for all stations using cell concentrations and a carbon per cell ratio as detailed in the materials and methods section (Table 3). *Synechococcus* contributed 3.3 to 67.7% to the total phytoplankton biomass, with the lowest contribution at station 17 (cyclonic gyre) and the highest south of Cyprus (station 74, Shikmona anticyclone). The *Synechococcus* contribution was also very high in the Ierapetra anticyclone (45.7%, station 47). *Prochlorococcus* contributed weakly to the total phytoplanktonic biomass (from 0.5% at the Sicily Strait to 6.5% at station 24 influenced by the cyclonic eddy).

3.3 Meso-scale dynamics and ultraphytoplankton distribution

Ultraphytoplankton vertical distributions were investigated in some details in those regions that were dynamically active, exhibiting relatively higher phytoplankton abundances even though locally limited.

3.3.1 Southern Adriatic

Figure 6a shows the vertical distribution of temperature, salinity and density in the southern Adriatic. Typical aspects of winter convection are shown at station 17 located in the centre of the cyclonic gyre, where uniform hydrographic properties ($t \approx 13.25$°C, $S \approx 38.65$, and density ≈ 29.18 kg m^{-3}) in the top 0–400 m clearly attest the extent of the convective mixing of the water column; in contrast, 40 km far from the centre of the gyre (stations 16 and 19), a thermohaline stratification persists because of the strong gradient between the relative fresh water from the northern regions and the LIW entrained in the cyclonic circulation pattern, as illustrated in Fig. 3c. It is worthy to notice the thermal inversion with depth through the 50 and 150 m levels; the vertical stability of the water column is maintained by the salinity. Thus, three water masses can be distinguished in the upper 200 m layer: (i) the relatively fresh waters of riverine input in the upper 50 m; (ii) the coldest and dense water from the northern shelf regions (50–100 m); and (iii) the transitional layer towards the warmer, saline intrusion of the much more dense LIW in the beneath. The eddy field shows that maximum salinity cores of LIW were trapped in the gyre, resulting in a vertical distribution of more saline waters at station 17, whilst the fresher and lighter waters of riverine input, mainly flowing from the northern Adriatic region, were entrained around the gyre (stations 16 and 19); these waters were transported to the south by the western Adriatic Costal Current (Artegiani et al., 1997), and might be traced as far as the Strait of Otranto (station 15).

In the southern Adriatic, the three ultraphytoplanktonic populations showed a uniform vertical distribution at the centre of the gyre (Fig. 6b) with low integrated abundances of about 3.4, 23.3 and 33.8×10^{10} cells m^{-2} for nanoeukaryotes, *Prochlorococcus* and *Synechococcus*, respectively. On the other hand, variable quantities towards higher integrated abundances were outside, at the periphery of the gyre (stations 16 and 19), and at the Otranto Strait (station 15). These patterns were very similar to the vertical nutrient distributions (not shown). Generally, the two sites are dynamically related by cyclonic circulation that causes the exchange of Adriatic/Ionian waters across the Strait

BGD
6, 6839–6887, 2009

(i.e. Adriatic Surface Waters to the west and Ionian Surface waters to the east that outflow/intrude into the Ionian/Adriatic basin) probably more intensely during the winter (Gacic et al., 1996).

In order to show the impact of the hydrodynamic structure, i.e. the cyclonic gyre in the southern Adriatic, on the abundance of ultraphytoplankton, we looked for a possible relationship between density and cell abundance where hydrodynamism is strong enough. Two stations can be considered affected by an hydrodynamic feature when densities values at a same depth and over a given depth range are different so that the slopes of the pycnoclines are very steep. With depth, the ratio of the density values at the compared stations tends toward one, which characterizes homogeneous deep layers. Considering station 17 in the core of the gyre and station 15 outside the gyre with a pycnocline at about 100 m depth, we found a significant linear relationship between the density ratio σ_{17}/σ_{15} and depth in the 50–150 m layer as illustrated by Fig. 7b. We also found a significant linear relationship in the 50–150 m column between depth and the natural logarithm of *Synechococcus* abundance ratio Syn_{17}/Syn_{15} as shown in Fig. 7a. A significant linear (r^2=0.91, p<0.01) correlation was found between abundance and density ratios: Syn_{17}/Syn_{15}=a (σ_{17}/σ_{15})+b (Fig. 7c). Relationships between pico- and nanoeukaryotes and depth or density were not significant (Table 4). At station 16, the pycnocline was shallower (30–40 m) and the significant relationship involving *Synechococcus* abundances at stations 17 and 16 took the form of a power function (Table 4). In that case, the similar relationships for pico- and nanoeukaryotes were significant (Table 4).

3.3.2 Eastern Ionian

The vertical distribution of the hydrographic measurements in the eastern Ionian was analyzed along the north-south transect defined by stations 24 to 29, which crosses the area where we observed eddy fields (Fig. 3). The vertical sections provide evidence of the formation of a thermohaline front located between stations 25 and 27 (Fig. 8). The front extended down to 200 m, separating two different water masses: (i) the cold and

more saline to the north stations (24 and 25), and (ii) the warmer and less saline to the south of the front (stations 27–29). It appears evident from these distributions that the space scales of the eddy were about 100 km; water mass analysis for this eddy fields shows that the LIW (i.e. a cold, more saline, poor in oxygen water mass with density of ≈28.85 kg m^{-3}) entrained in the cyclonic circulation and upwelled close to the photic layer, but no convective mixing occurred because of the strong pycnocline established by the density structure. On the other hand, minimum salinity cores of AW were trapped in the anticyclone found in the southern region. The chemical features of these water masses were also different. In particular, nitrate and silicate concentrations between 60 and 200 m depth were higher north of the front than south of it (not shown), while concentration of dissolved oxygen was lower in the north than in the south (Fig. 8d).

The impact of this thermohaline front on the vertical distribution of ultraphytoplankton is illustrated by Fig. 9. For pico- and nanoeukaryotes, the transition across the front resulted essentially in their deeper presence south of the front than at station 25, specially down to 100 m. In contrast, the vertical distributions of *Synechococcus* and *Prochlorococcus* were more affected by the front. Indeed, north of the front, the two distributions were complementary, *Synechococcus* occupying the upper 75 m and *Prochlorococcus* being present below, between 75 and 150 m, with about the same maximum concentration (≈20 000 cells cm^{-3}) whereas south of the front *Synechococcus* was present deeper (down to 150 m) and *Prochlorococcus* concentration decreased and dropped below 1000 cells cm^{-3} throughout the water column.

At station 25, the strong vertical variation of density between 60 and 75 m depth (Fig. 8c) was coupled to a large abundance decline for all ultraphytoplankton groups. At station 27 where the vertical variation of density was smoother (Fig. 8c), the ultraphytoplankton concentration declined more progressively with depth. We found a linear relationship between the ratio σ_{25}/σ_{27} of density values and depth between 75 and 200 m at stations 25 and 27 (Fig. 10b). We also found a significant linear relationship in the same depth range (75–200 m) between depth and the natural logarithm of *Synechococcus* abundance ratio Syn_{25}/Syn_{27} as shown in Fig. 10a. A significant

BGD
6, 6839–6887, 2009

(r^2=0.89, p<0.05) correlation between abundance and density ratios: $Syn_{25}/Syn_{27}=a(\sigma_{25}/\sigma_{27})+b$ was also found as shown in Fig. 12c. Similar relationships between depth and density or abundance ratios and between abundance ratios and density for pico- and nanoeukaryotes were not significant (Table 4).

3.3.3 Transition from the eastern to the western Mediterranean

Differences between the eastern and western Mediterranean were provided by stations sampled on both sides of the Sicily Strait, along the transect made by stations 2 to 10. Indeed, the physical features of the water masses varied between stations 5 and 7 when crossing the Sicily Strait that makes the geographical separation between the western and eastern Mediterranean. Temperature and salinity in the surface layer were homogeneous west of the Sicily Strait and increased significantly in the eastern side of the transect, from 15.5 to 17.0°C and from 37.50 to 38.25, respectively (Fig. 11). In the upper 200 m, nitrate and silicate concentrations largely decreased eastwards (not shown). For instance, surface concentrations of nitrate decreased from about 0.7 μM to undetectable levels and, at 200 m, from 2–7 μM to <1.4 μM. In contrast, dissolved oxygen concentrations were relatively homogeneous on both sides of the Sicily Strait, decreasing with depth from 245 μM between 0–100 m to about 200 μM at 200 m.

Nanoeukaryotes were mainly present in the upper 80 m, with abundances slightly decreasing eastwards from about 400 to 300 cells cm^{-3} (Fig. 12a). Picoeukaryotes were more abundant in the western Mediterranean with a maximum value of 3000 cells cm^{-3} at 40 m depth, station 2 (Fig. 12b). At station 7, in the eastern Mediterranean, picoeukaryote abundance was weaker (≈1000 cells cm^{-3}) and homogeneously distributed over the upper 100 m. This abundance declined continuously further east. *Prochlorococcus* presented a contrasted distribution on both sides of the Sicily Strait, mainly occupying the upper 70 m on the west side, with abundances >2000 cells cm^{-3}, whereas on the east side, abundances in the upper 70 m were <1000 cells cm^{-3}, but were maximum at 100 m with values close to 4000 cells cm^{-3} (Fig. 12c). *Synechococ-*

BGD
6, 6839–6887, 2009

cus abundance was high at surface and decreased with depth (Fig. 12d). The peculiarity is that its abundance was higher in the eastern Basin (10 000 cells cm^{-3} at station 11) than in the western Basin (6000 cells cm^{-3} stations 2 to 5). In addition, the occupied layer was more important on the east side of the Sicily Strait (0–80 m) than on the west side (<40 m).

The comparison of the eastern and western Mediterranean does not directly involve hydrodynamic structures but rather water masses with different properties. The surface of the western Mediterranean under the influence of the Atlantic water inflow is less saline than the eastern Mediterranean where evaporation is a major feature. Considering stations 5 and 7 as representative of both sides of the Sicily Strait, and salinity as the driving factor, we found a linear relationship between depth and the ratio S_7/S_5 of salinity values from the same depths at stations 5 and 7. This relationship applies to the 75–150 m depth range as illustrated by Fig. 13a together with the vertical distribution of salinity at both stations in the same depth range (Fig. 16b). We also found a significant linear relationship in the same depth range between depth and the picoeukaryote abundance ratio $Pico_5/Pico_7$ as shown in Fig. 13c. From both relationships, we derived a significant (r^2=0.88, p<0.05) correlation between both abundance and salinity ratios: $Pico_7/Pico_5 = a\,Ln(S_7/S_5)+b$ (Fig. 13d). A similar relationship was significant (r^2=0.75, p<0.05) for nanoeukaryotes but not significant for *Synechococcus* (Table 4).

4 Discussion

Phytoplankton distribution in the eastern Mediterranean has been poorly documented until the recent years. Only few spatially limited investigations of ultraphytoplankton abundances corresponding to different periods were reported in the literature (Li et al., 1993; Yacobi et al., 1995; Zohary et al., 1998, Psarra et al., 2005). The only synoptic study related to phytoplankton, to our knowledge, was that derived from ocean color data (CZCS) conducted by Antoine et al. (1995) and dedicated to chlorophyll and primary production. The METEOR 31/1 cruise (January 1995) provided support for the

first basin-scale field-study of phytoplankton distribution in the eastern Mediterranean. Thus a basin-wide winter phytoplankton pigment distribution in the eastern Mediterranean, conducted during this cruise, was reported (Vidussi et al.,2001). In parallel the study presented here reports the first basin-wide spatial distribution of ultraphytoplankton (<10 μm) determined by flow cytometry. Since then, further flow cytometry studies in the eastern Mediterranean at a few sites were achieved in springtime on picophytoplankton (Moutin et al., 2002) or in summer on ultraphytoplankton (Psarra et al., 2005) and on ultraphytoplankton distribution exclusively in the Ionian basin (Casotti et al., 2003).

The dominance of picoeukaryotes over nanoeukaryotes reported in this study reflects the general oligotrophic status of the eastern Mediterranean even during the winter season as evidenced by the Rpn index (Denis et al., 2003). This index, which was proposed for the first time during a study on the transition from mesotrophy to oligotrophy observed in western Mediterranean is defined by the abundance ratio picoeukaryotes/nanoeukaryotes and characterizes the mesotrophic (Rpn<1) or oligotrophic (Rpn>1) status of an ecosystem. The carbon biomass estimations showed that *Synechococcus* contributed 3.3% to 67.7% to the overall phytoplanktonic biomass in the eastern Mediterranean (Table 3). In contrast, *Prochlorococcus* contributed far less, from 0.5% to 6.5. *Synechococcus* represented more than 20% of the overall phytoplankton biomass at the majority of sampled stations. The mean integrated carbon biomasses of pico- and nanoeukaryotes (168 and 681 mg C m^{-2}, respectively) are in agreement with mean values derived from their integrated chl a biomasses (270 and 630 mg C m^{-2}, respectively) as reported by Vidussi et al. (2001) when using the Carbon/chla conversion factor of 50 (Brown et al., 1999). The choice of this ratio is consistent with the ratio value of 55 obtained from data assimilation modelling in the north western Mediterranean (Faugeras et al., 2003) and with the ratio value of 47 obtained from an experimental approach in the same region (Latasa et al., 2005). The distribution maps (Fig. 5) of integrated (0–200 m) abundances of the four resolved ultraphytoplanktonic clusters show that their distribution was not uniform over the eastern

Mediterranean where *Synechococcus* was the dominant species. However, its maximum abundance (about 37 000 cells cm^{-3}) was 26% less than the winter maximum concentration (about 50 000 cells cm^{-3}) reported for the western Mediterranean (Vaulot et al., 1990). In the western Mediterranean, the presence of *Prochlorococcus* in the top layer was consistent with the observations of Vaulot et al. (1990). Contrary to other oligotrophic ocean regions, where *Prochlorococcus* dominate the picophytoplankton fraction (see review of Partensky et al., 1999, and references therein), the dominance of *Synechococcus* during this study supports the suggestion that *Synechococcus* would be more adapted than *Prochlorococcus* to the hydrodynamical and nutrient conditions of the eastern Mediterranean. Different hypothesis can be proposed to explain the *Synechococcus* dominance in the oligotrophic eastern Mediterranean as the nitrogen-fixation capacity of the strain present in the eastern Mediterranean, like those detected in oligotrophic oceans (Zehr et al., 1998). However, direct evidence of the Mediterranean *Synechococcus* strain capacity for nitrogen-fixation is still lacking. The winter mixing can also partly explain the dominance of *Synechococcus* over *Prochlorococcus* in the eastern Mediterranean (Partensky et al., 1999). The absence of fluorescence increase with depth for *Synechococcus* and for the pico and nanoeukaryotic phytoplankton was reasonably due to large mixed layer depths induced by winter conditions. For instance, the mixed layer depth reached 400 m in the Adriatic (Fig. 6). Under these conditions, *Prochlorococcus* mean fluorescence per cell provided evidence for the presence of two ecotypes along the water column, one occupying the upper 75 m, the other, adapted to low light, growing preferentially below 75 m in agreement with previous reports (Vaulot et al., 1990; Partensky et al., 1999). These ecotypes would also combine adaptation to the availability of nitrogen sources (nitrate, nitrite and ammonium; Moore et al., 2002). The existence of three ecotypes of *Prochlorococcus* in equatorial Pacific was reported (Mackey et al., 2002), however no evidence for a third species could be derived from our data. We must mention that the ecotype adapted to high light was likely underestimated in our measurements due to its low fluorescence level.

BGD
6, 6839–6887, 2009

This study provides clear examples of the dependence of ultraphytoplankton spatial distribution on meso or sub-meso scale hydrodynamic features. In the Adriatic, the inside waters of the observed cyclonic gyre were very homogeneous in the upper 400 m in contrast with outside waters (Fig. 6a), and their ultraphytoplankton content was significantly lower than at the edge of the gyre or in surrounding waters (Fig. 6b). *Synechococcus* distribution was the most affected by the presence of the gyre. Inside the gyre, the upward movement of waters resulted in a uniform density distribution with depth (Fig. 6a), whereas outside the gyre, density increased with depth, continuously approaching the value inside the gyre. The *Synechococcus* concentration exhibited a pattern reflecting the hydrodynamic features. To account for the ultraphytoplankton distribution outside the gyre, we speculate upon possible mechanisms of water mass transport from the northern region including patches of high quantities of ultraphytoplankton and/or locally lived and advected from offshore stations. The linear relationships found between *Synechococcus* abundance and density inside and outside the gyre, express a tight control of *Synechococcus* by the density, at least in the depth range between 50 and 150 m (Fig. 7c). In the upper layer, additional factors such as light, predation and nutrients would contribute to a more complex relationship between *Synechococcus* abundances inside and outside the gyre.

In the Ionian basin, the presence of a thermohaline front (Fig. 8) mainly modified the vertical distribution of both *Synechococcus* and *Prochlorococcus*. North of the front, where waters were colder and more saline than south of the front, both genera appeared complementary with *Synechococcus* restricted to the upper 75 m and *Prochlorococcus* being as abundant below (Fig. 9). South of the front, *Prochlorococcus* abundance dropped to its background level below 75 m and was replaced by *Synechococcus*. The thermohaline front was also responsible for the density variations between stations 25 and 27 (Fig. 8). The large density change between 60 and 75 m depth at station 25 was coupled to a large drop in *Synechococcus* concentration (Fig. 9). In contrast, at station 27, the vertical variation of density was less pronounced and the *Synechococcus* concentration decreased more progressively. Below

BGD
6, 6839–6887, 2009

50 m depth, the ratios of cell concentrations and density between stations 25 and 27 provide evidence of a phasing in the concentration decrease with depth and of a pycnocline (ratio tending towards 1), expressing the impact of the front (Fig. 10). Both ratios were found significantly correlated (Fig. 10c). Ultraphytoplankton concentrations were larger above the pycnocline than below whereas density became rapidly homogeneous below the pycnocline.

In the comparison of western and eastern Mediterranean, the considered changes are related to salinity, not to a local hydrodynamic system. Though salinity explains the variations in picophytoplankton distributions (Fig. 13) according to relationships analogous to those found for the frontal system in the Ionian basin, the interpretation might not be as straightforward due to the large space scale covered.

The impact of environmental changes induced by the considered hydrodynamic features was found significant on the most abundant cluster but not on the less populated group. This suggests that a cluster must be abundant enough to play a role of bioindicator for changes in the environmental conditions. This property should deserve attention in the study of microbial ecosystems for instance.

As the first investigation of ultraphytoplankton winter distribution in the eastern Mediterranean, the present study will significantly contribute to a better knowledge of the ultraphytoplankton structure over seasons and of its dependence on hydrological features. It also provides evidence for the sensitivity of the different ultraphytoplankton clusters to changes in their environmental conditions.

Acknowledgements. This work was partially supported by the CNRS-INSU and the GEODYME project (contract No. 930061 of the MTP-MAST II programme). We thank the captain and crew of the R. V. Meteor for their efficient assistance at sea. W. Roether is especially acknowledged for the opportunity of taking part to the Meteor cruise. We are very grateful to J. P. Béthoux, coordinator of the GEODYME project, for his stimulating support during this study.

The publication of this article is financed by CNRS-INSU.

References

Antoine, D., Morel, A., and André, J.-M.: Algal pigment distribution and primary production in the eastern Mediterranean as derived from coastal zone color scanner observations, J. Geophys. Res., 100, 16193–16209, 1995.

Artegiani, A., Bregant, D., Paschini, E., Pinardi, N., Raicich, F., and Russo, A.: The Adriatic Sea general circulation. Part II: baroclinic circulation structure, J. Phys. Oceanogr., 27, 1515–1532, 1997.

Azov, Y.: Seasonal patterns of phytoplankton productivity and abundance in nearshore oligotrophic waters of Levant Basin (Mediterranean), J. Plankt. Res., 8, 41–53, 1986.

Berland, B.: Azote ou phosphore ? Considérations sur le "paradoxe nutritionnel" de la mer Méditerranée, Oceanol. Acta, 3, 135–142, 1980.

Berman, T., Townsend, D. W., El-Sayed, S. Z., Trees, C. C., and Azov, Y.: Optical transparency, chlorophyll and primary productivity in the eastern Mediterranean near the Israeli coast, Oceanol. Acta, 7, 367–372, 1984.

Béthoux, J. P.: Budgets of the Mediterranean Sea. Their dependance on the local climate and on characteristics of the Atlantic waters, Oceanol. Acta, 2, 157–163, 1979.

Bonin, D. J., Bonin, M. C., and Berman, T.: Mise en évidence expérimentale des facteurs nutritifs limitants de la production du micro-nanoplancton et de l'ultraplancton dans une eau côtière de la Méditerranée orientale (Haïfa, Israël), Aquat. Sci., 51, 129–152, 1989.

Brown, S. L., Landry, M. R., Barber, R. T., Campbell, L., Garrison, D. L., and Gowing, M. M.: Picophytoplankton dynamics and production in the Arabian Sea during the 1995 southwest monsoon, Deep-Sea Res. II, 46, 1745–1768, 1999.

Cailliau, C., Claustre, H., Vidussi, F., Marie, D., and Vaulot, D.: Carbon biomass, and

gross growth rates as estimated from 14C pigment labelling, during photoacclimatation in *Prochlorococcus* CCMP 1378, Mar. Ecol. Prog. Ser., 145, 209–211, 1996.
Carter, E. F. and Robinson, A. R.: Analysis models for estimation of ocean fields, J. Atmos. Ocean Technol., 4, 49–74, 1987.
Casotti, R., Landolfi, A., Brunet, C., D'Ortenzio, F., Mangoni, O., Ribera d'Alcalà, M., and Denis, M.: Composition and dynamics of the phytoplankton of the Ionian Sea (eastern Mediterranean), J. Geophys. Res., 108:PBE17-1, 17–19, 2003.
Claustre, H., Kerhervé, P., Marty, J.-C., Prieur, L., Videau, C., and Hecq, J.-H.: Phytoplankton dynamics associated with a geostrophic front: ecological and biogeochemical implications, J. Mar. Res., 52, 711–742, 1994.
Conan, P., Pujo-Pay, M., Raimbault, P., and Leveau, M.: Variabilité hydrologique et biologique du golfe du Lion, II. Productivité sur le bord interne du courant, Oceanol. Acta, 21, 767–782, 1998.
De Boyer Montégut, C., Madec, G., Ficher, A. S., Lazar, A., and Iudicone, D.: Mixed layer depth over the global ocean: An examination of profile data and a profile-based climatology, J. Geophys. Res., 109, C12003, doi:10.1029/2004JC002378, 2004.
Denis, M., Martin, V., and Andersen, V.: Short-term variations of the vertical distribution of cyanobacteria in the open Mediterranean Sea, Sci. Mar., 64, 157–163, 2000.
Denis, M., Martin, V., Momzikoff, A., Gondry, G., Stemmann, L., Demers, S., Gorsky, G., and Andersen, V.: Pulsed remineralisation in the north western Mediterranean Sea: an hypothesis, J. Mar. Syst., 39, 19–41, 2003.
Faugeras, B., Lévy, M., Mémery, L., Verron, J., Blum, J., and Charpentier, I.: Can biogeochemical fluxes be recovered from nitrate and chlorophyll data? A case study assimilating data in the north western Mediterranean Sea at the JGOFS-DYFAMED station, J. Mar. Syst., 40–41, 99–125, 2003.
Gacic, M., Kovacevich, V., Manca, B., Papageorgiou, E., Poulain, P. M., Scarazzato, P., and Vetrano, A.: Thermohaline properties and circulation in the Strait of Otranto, in: Dynamics of Mediterranean Straits and Channels, edited by: Briand, F., Bul. Inst. Oceanogr., Special Issue, 17, CIESM Science Series, 2, 117–145, 1996.
Klein, B., Roether, W., Manca, B. B., Bregant, D., Beitzel, V., Kovacevich, V., and Luchetta, A.: The large deep water transient in the eastern Mediterranean, Deep-Sea Res. I, 46, 371–414, 1999.
Krom, M. D., Kress, N., Brenner, S., and Gordon, L. I.: Phosphorus limitation of primary pro-

ductivity in the eastern Mediterranean, Limnol. Oceanogr., 36, 424–432, 1991.
Krom, M. D., Brenner, S., Kress, N., Neori, A., and Gordon, L. I.: Nutrient dynamics and new production in a warm-core eddy from the eastern Mediterranean Sea, Deep-Sea Res., 39, 467–480, 1992.
Krom, M. D., Brenner, S., Kress, N., Neori, A., and Gordon, L. I.: Nutrient distributions during an annual cycle across a warm-core eddy from the E. Mediterranean Sea, Deep-Sea Res., 40, 805–825, 1993.
Krom, M. D., Groom, S., and Zohary, T.: The eastern Mediterranean, in: The Biogeochemistry of Marine Systems, edited by: Black, K. D. and Shimmield, G. B., Blackwell Publishing Oxford, pp. 916 126, 2003.
Krom, M. D., Thingstad, T. F., Brenner, S., Carbo, P., Drakopoulos, P., Fileman, T. W., Flaten, G. A. F., Groom, S., Herut, B., Kitidis, V., Kress, N., Law, C. S., Liddicoat, M. I., Mantoura, R. F. C., Pasternak, A., Pitta, P., Polychronaki, T., Psarra, S., Rassoulzadegan, F., Skjoldal, E. F., Spyres, G., Tanaka, T., Tselepides, A., Wassmann, P., Wexels Riser, C., Woodward, E. M. S., Zodiatis, G., and Zohary, T.: Summary and overview of the CYCLOPS P addition Lagrangian experiment in the eastern Mediterranean, Deep-Sea Res. Part II, 52, 3090–3108, 2005.
Latasa, M., Moran, X. A. G., Scharek, R., and Estrada, M.: Estimating the carbon flux through main phytoplankton groups in the north western Mediterranean, Limnol. Oceanogr., 50 1447–1458, 2005.
Leaman, K. D. and Schott, F. A.: Hydrographic structure of the convection regime in the Gulf of Lions: Winter 1987, J. Phys. Oceanogr., 21, 575–598, 1991.
Li, W. K. W., Zohary, T., Yacobi, Y. Z., and Wood, A. M.: Ultraphytoplankton in the eastern Mediterranean Sea: towards deriving phytoplankton biomass from flow cytometric measurements of abundance, fluorescence and light scatter, Mar. Ecol. Prog. Ser., 102, 79–87, 1993.
LIWEX, Group: The Levantine Intermediate Water Experiment (LIWEX) Group: Levantine basin – A laboratory for multiple water mass formation processes, J. Geophys. Res., 108, 8101, doi:10.1029/2002JC001643, 2003.
Mackey, D. J., Blanchot, J., Higgins, H. W., and Neveux, J.: Phytoplankton abundances and community structure in the equatorial Pacific, Deep-Sea Res. Part II, 49, 2561–2582, 2002.
Malanotte-Rizzoli, P., Manca, B. B., Ribera d'Alcalà, M., Theocharis, A., Brenner, S., Budillon, G., and Ozsoy, E.: The eastern Mediterranean in the 80s and in the 90s: the big transition in the intermediate and deep circulations, Dyn. Atmos. Oceans, 29, 365–395, 1999.
Martin, V.: Etude par cytométrie en flux de la distribution des populations phytoplanctoniques

BGD
6, 6839–6887, 2009

en Méditerranée, Mise en relation avec la production métabolique de CO_2 et comparaison avec le Golfe du Saint Laurent, Thesis, Université de la Méditerranée, 250 p., 1997.
Marty, J.-C., Chiavérini, J., Pizay, M.-D., and Avril, B.: Seasonal ad interannual dynamics of nutrients and phytoplankton pigments in the western Mediterranean Sea at the DYFAMED time-series station (1991–1999), Deep-Sea Res. Part II, 49, 1965–1985, 2002.
Minas, H. J., Minas, M., Coste, B., Gostan, J., Nival, P., and Bonin, M.-C.: Production de base et de recyclage; une revue de la problématique en Méditerranée nord-occidentale, in: Oceanol. Acta, Océanologie pélagique méditerranéenne, edited by: Minas, H. J. and Nival, P., 155–162, 1988.
Moore, L. R., Post, A. F., Rocab, G., and Chisholm, S. W.: Utilization of different nitrogen sources by marine cyanobacteria *Prochlorococcus* and *Synechococcus*, Limnol. Oceanogr., 47, 989–996, 2002.
Moutin, T., Thingstad, T.F., Van Wambeke, F., Marie, D., Slawyk, G., Raimbault, P., and Claustre, H.: Does competition for nano-molar phosphate supply explain the predominance of the cyanobacterium *Synechococcus*?, Limnol. Oceanogr., 47, 1562–1567, 2002.
Partensky, F., Hess, W. R., and Vaulot, D.: *Prochlorococcus*, a marine photosynthetic prokaryote of global significance, Microbiol. Mol. Biol. Rev., 63, 106–127, 1999.
Platt, T., Subba Rao, D. V., and Irvin, B.: Photosynthesis of picoplankton in the oligotrophic ocean, Nature, 301, 702–704, 1983.
POEM group: The general circulation of the eastern Mediterranean, Earth Sci. Rev., 32, 285–309, 1992.
Psarra, S., Tselepides, A., and Ignatiades, L.: Primary productivity in the Cretan Sea (NE Mediterranean):seasonal and interannual variability, Prog. Oceanogr., 46, 187–204, 2000.
Psarra, S., Zohary, T., Krom, M. D., Mantoura, R. F. C., Polychronaki, T., Stambler, N., Tanaka, T., Tselepides, A., and Thingstad, T. F.: Phytoplankton response to a Lagrangian phosphate addition in the Levantine Sea (eastern Mediterranean), Deep-Sea Res. Part II, 52, 2944–2960, 2005.
Rodriguez, J., Tintore, J., Allen, J. T., Blanco, J. M., Gomis, D., Reul, A., Ruiz, J., Rodriguez, V., Echevarria, F., and Rodriguez, F. J.: Mesoscale vertical motion and the size structure of phytoplankton in the ocean, Nature, 410, 360–363, 2001.
Roether, W., Manca, B. B., Klein, B., Bregant, D., Georgopoulos, D., Beitzel, V., Kovacevich, V., and Luchetta, A.: Recent changes in eastern Mediterranean deep waters, Science, 271, 333–335, 1996.

Roussenov, V., Stanev, E., Artale, V., and Pinardi, N.: A seasonal model of the Mediterranean Sea general circulation, J. Geophys. Res., 100, 13515–13538, 1995.
Schlitzer, R., Roether, W., Oster, H., Junghans, H.-G., Hausmann, M., Johannsen, H., and Michelato, A.: Chlorofluoromethane and oxygen in the eastern Mediterranean, Deep-Sea Res., 38, 1531–1551, 1991.
Thingstad, T. F., Krom, M. D., Mantoura, R. F. C., Flaten, G. A. F., Groom, S., Herut, B., Kress, N., Law, C. S., Pasternak, A., Pitta, P., Psarra, S., Rassoulzadegan F., Tanaka, T., Tselepides, A., Wassmann, P. Woodward, E. M. S., Wexels, Riser, C., Zodiatis, G., and Zohary, T.: Nature of phosphorus limitation in the ultraoligotrophic eastern Mediterranean, Science, 309, 1068–1071, 2005.
Tselepides, A., Zervakis, V., Polychronaki, T., Donavaro, R., and Chronis, G.: Distribution of nutrients and particulate organic matter in relation to the prevailing hydrographic features of the Cretan Sea (NE Mediterranean), Prog. Oceanogr., 46, 113–142, 2000.
Trousselier, M., Courties, C., and Zettlemaier, S.: Flow cytometric analysis of coastal lagoon bacterioplankton and picoplankton: fixation and storage effects, Est. Coast. Shelf Res., 40, 621–623, 1995.
Van Wambeke, F., Christaki, U., Giannakourou, A., Moutin, T., and Souvemerzoglou, K.: Longitudinal and vertical trends of bacterial limitation by phosphorus and carbon in the Mediterranean Sea, Microb. Ecol., 43, 119–133, 2002.
Vaulot, D., Courties, C., and Partensky, F.: A simple method to preserve oceanic phytoplankton for flow cytometric analyses, Cytometry, 10, 629–635, 1989.
Vaulot, D., Partensky, F., Neveux, J., Mantoura, R. F. C., and Llewellyn, C. A.: Winter presence of prochlorophytes in surface waters of the north western Mediterranean Sea, Limnol. Oceanogr., 35, 1156–1164, 1990.
Vaulot, D., LeBot, N., Marie, D., and Fukai, E.: Effect of phosphorus on the *Synechococcus* cell cycle in surface Mediterranean waters during summer, Appl. Environ. Microbiol., 62, 2527–2533, 1996.
Verity, P. G., Robertson, C.Y., Tronzo, C. R., Andrews, M. G., Nelson J. R., and Sieracki, M. E.: Relationships between cell volume and the carbon and nitrogen content of marine photosynthetic nanoplankton, Limnol. Oceanogr., 37, 1434–1446, 1992.
Vidussi, F., Claustre, H., Bustillo-Guzman, J., Caillau, C., and Marty, J.-C.: Determination of chlorophylls and carotenoids of marine phytoplankton. Separation of chlorophyll a from divinyl-chlorophyll a and zeaxanthin from lutein, J. Plankt. Res., 18, 2377–2382, 1996.

Vidussi, F., Claustre, H., Manca, B. B., Luchetta, A., and Marty, J.-C.: Phytoplankton pigment distribution in relation to upper thermocline circulation in the eastern Mediterranean Sea during winter, J. Geophys. Res., 106, 19939–19956, 2001.

Waterbury, J. B., Watson, S. W., Valois, F. W., and Franks, D. G.: Biological and ecological characterization of the marine unicellular cyanobacterium *Synechococcus*, in: Photosynthetic picoplankton, edited by: Platt, T. and Li, W. K. W., Can. Bul. Fish. Aquat. Sci., 71–120, 1986.

Wüst, G.: On the vertical circulation of the Mediterranean Sea, J. Geophys. Res., 66, 3261–3271, 1961.

Yacobi, Y. Z., Zohary, T., Kress, N., Hecht, A., Robarts, R. D., Waiser, M., Wood, W., and Li, W. K. W.: Chlorophyll distribution throughout the southeastern Mediterranean in relation to the physical structure of water mass, J. Mar. Syst., 6, 179–190, 1995.

Zehr, J. P., Mellon, M. T., and Zani, S.: New nitrogen-fixing microorganisms detected in oligotrophic oceans by amplification of nitrogenase (nifH) genes, Appl. Environ. Microbiol., 64, 3444–3450, 1998.

Zehr, J. P., Waterbury, J. B., Turner, P. J., Montoya, J. P., Omoregie, E., Steward, G. F., Hansen, A., and Karl, D. M.: Unicellular cyanobacteria fix N_2 in the subtropical north Pacific Ocean, Nature, 412, 635–638, 2001.

Zohary, T., Brenner, S., Krom, M.D., Angel, D. L., Kress, N., Li, W. K. W., Neori, A., and Yacobi, Y. Z.: Buildup of microbial biomass during deep winter mixing in a Mediterranean warm-core eddy, Mar. Ecol. Progr. Ser., 167, 47–57, 1998.

Zohary, T. and Robarts, R. D.: Experimental study of microbial P-limitation in the eastern Mediterranean, Limnol. Oceanogr., 43, 387–395, 1998.

Zohary, T., Herut, B., Krom, M. D., Fauzi, R., Mantoura, C., Pitta, P., Psarra, S., Rassoulzadegan, F., Stambler, N., Tanaka, T., Thingstad, T. F., and Woodward, E. M. S.: P-limited bacteria but N and P co-limited phytoplankton in the eastern Mediterranean – a microcosm experiment, Deep-Sea Res. Part II, 52, 3011–3023, 2005.

Table 1. MLD calculated from a threshold method at which changes in density from that at the reference depth of 2 m are greater than the threshold value ($\Delta\sigma_\theta$) as indicated.

Western Ionian			Eastern Ionian			South Adriatic		
Station	$\Delta\sigma_\theta$ kg m^{-3}	MLD m	Station	$\Delta\sigma_\theta$ kg m^{-3}	MLD m	Station	$\Delta\sigma_\theta$ kg m^{-3}	MLD m
5	0.02	98	24	0.02	68	15	0.05	83
6	0.02	66	25	0.02	60	16	0.05	39
7	0.02	94	26	0.05	34	17	0.02	463
8	0.02	58	27	0.05	71	18	0.02	92
			28	0.02	103	19	0.02	101
			29	0.02	111			

BGD
6, 6839–6887, 2009

Table 2. Range of variation of the integrated biomasses of the different ultraphytoplankton groups in the Eastern Mediterranean. Maximum and minimum biomass values are associated with the stations where they have been observed.

		Biomass mg C m^{-2}	Station
Nanoeukaryotes	Max	1763.1	57
	Min	202.4	9
Picoeukaryotes	Max	453.3	34
	Min	18.2	49
Prochlorococcus	Max	57.6	24
	Min	9.1	44
Synechococcus	Max	571.2	47
	Min	67.7	17

BGD
6, 6839–6887, 2009

Table 3. Percentage of contribution of *Synechococcus* and *Prochlorococcus* to the overall chlorophyll *a* biomass. To calculate these contributions, chl *a* was expressed in terms of carbon biomass by using the ratio C/chl *a*=50.

Station	% of contribution to chl *a* biomass		Station	% of contribution to chl *a* biomass	
	Synechococcus	*Prochlorococcus*		*Synechococcus*	*Prochlorococcus*
2	9.5	1.5	32	20.0	1.2
3	4.6	0.9	33	15.0	1.2
4	6.1	1.4	34	14.7	1.1
5	5.9	0.5	36	23.1	1.1
7	14.5	1.3	38	31.4	2.2
8	29.6	2.1	40	17.3	1.9
9	25.5	1.6	41	6.9	1.3
10	34.8	2.5	43	14.4	1.7
11	32.7	1.9	44	11.7	0.8
14	20.6	2.4	47	45.7	1.3
15	20.9	3.0	49	35.6	1.9
16	22.3	1.7	50	24.5	2.2
17	3.3	0.6	51	36.7	1.5
19	17.1	0.9	54	21.2	0.7
20	14.7	1.6	55	10.9	2.2
21	22.1	1.9	57	17.3	1.3
23	27.6	1.7	58	6.6	1.3
24	28.3	6.5	61	15.1	1.2
25	22.9	4.5	62	22.8	1.5
27	30.4	1.8	69	18.6	2.5
28	38.4	2.0	71	24.3	1.3
29	36.0	3.2	73	25.2	3.5
30	33.3	1.6	74	67.7	2.7
31	31.3	1.6			

Table 4. Correlation coefficients (R^2) of linear relationships between ratios at a given depth (z_i) below 50 m of cell abundance $A(z_i)$ and density excess $\sigma(z_i)$ or salinity $S(z_i)$ at two compared stations. Linear relationships were also established between depth and the ratio of density excess or salinity at the two compared stations. The compared stations and the range of depth where the linear relationships were established are given in the first column. The linear relationships are explicitely written for stations 25 and 27 as an example.

		$A_{25}(z_i)/A_{27}(z_i)$=a*$\sigma_{25}(z_i)/\sigma_{27}(z_i)$+b			z=a*σ_{25}(z)/σ_{27}(z)+b	z=a*$S_{25}(z)$/S_{27}(z)+b
	n	*Synechoccocus*	Picoplantkon	Nanoplankton		
st 25–27 (85–200 m)	6	0.89*	0.68	0.08	0.96**	
st 16–17 (50–200 m)	6	0.80*	0.83*	0.79*	0.92**	
st 15–17 (50–200 m)	6	0.92**	0.52	0.47	0.92**	
		$A_{25}(z_i)/A_{27}(z_i)$=a*$S_{25}(z_i)/S_{27}(z_i)$+b				
st 5–7 (50–200 m)	6	0.3	0.88*	0.75*	0.45	0.81*

*p<0.05** p<0.01

BGD
6, 6839–6887, 2009

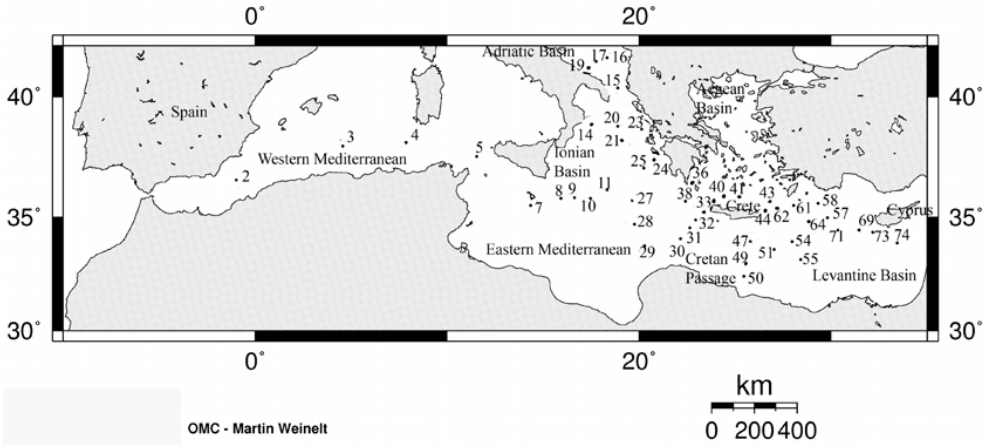

Fig. 1. Location of the stations during the METEOR cruise M31/1 (30 December 1994 to 5 February 1995) conducted in the Mediterranean sea in the frame of the POEM/BC (Physical Oceanography of the eastern Mediterranean – Biology, Chemistry) and the EU/MAST-MTP (Marine Science and Technology-Mediterranean Targeted Project) of the European Union programme.

BGD
6, 6839–6887, 2009

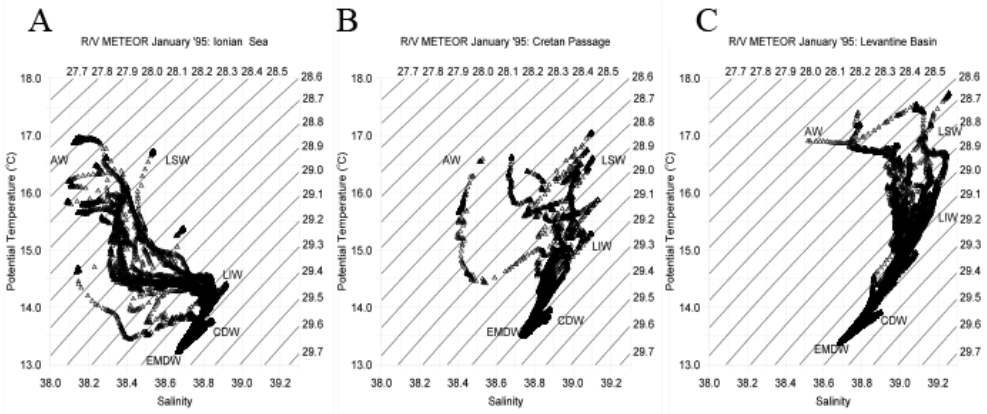

Fig. 2. θ/S Diagrams with CTD casts in the **(a)** Ionian Sea (stations 7–14 and 20–29), **(b)** Cretan Passage (stations 30–34 and 44–51), and **(c)** in the Levantine basin (stations 52–77). The different water types discussed in the text are indicated by their acronyms. AW: Atlantic water; LIW: Levantine intermediate water; LSW: Levantine surface water; CDW: Cretan deep water; EMDW: eastern Mediterranean deep water.

BGD
6, 6839–6887, 2009

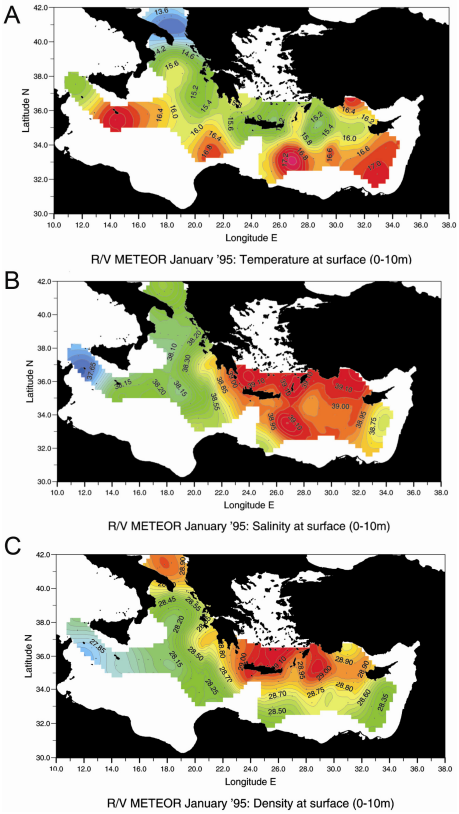

Fig. 3. Horizontal distribution of **(a)** temperature, **(b)** salinity and **(c)** density in the surface layer (data averaged over the interval 0–10 m) in January 1995.

BGD
6, 6839–6887, 2009

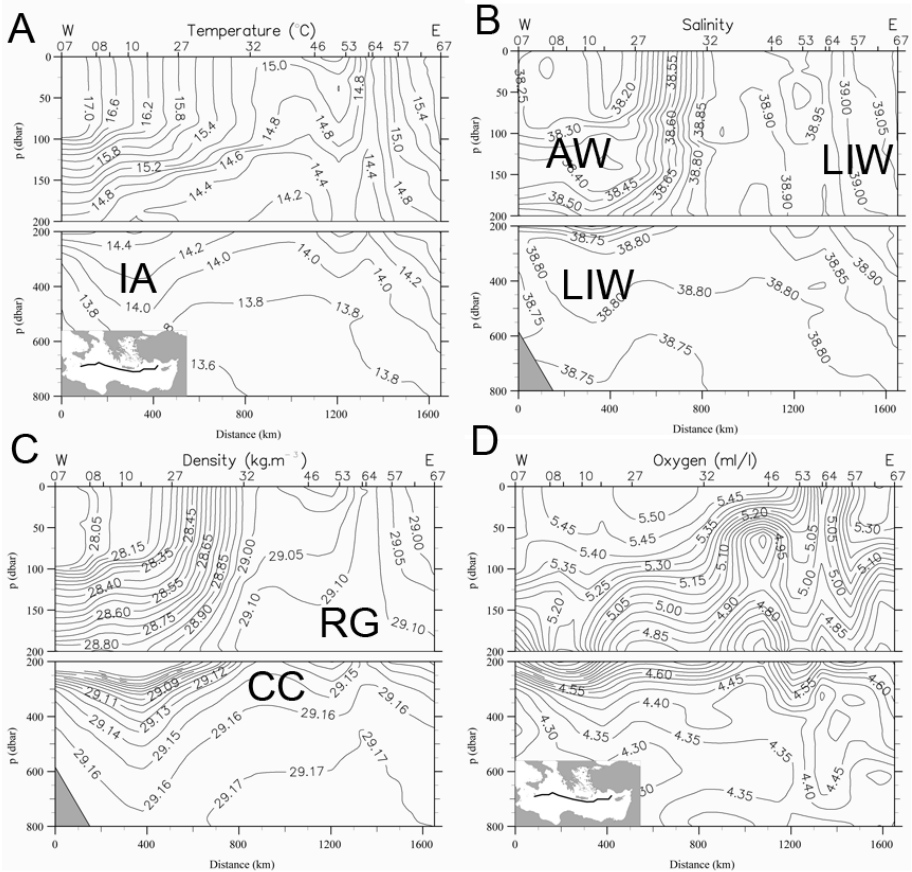

Fig. 4. Vertical distribution of **(a)** temperature, **(b)** salinity, **(c)** density, and **(d)** dissolved oxygen down to 800 m along the cross section through the eastern Mediterranean (see inset map) in January 1995. The position of the CTD stations is indicated at the top x axis. The positions of the Ionian Anticyclone (IA), the Cretan Cyclone (CC) and the Rhodes Gyre (RG) are also indicated.

BGD
6, 6839–6887, 2009

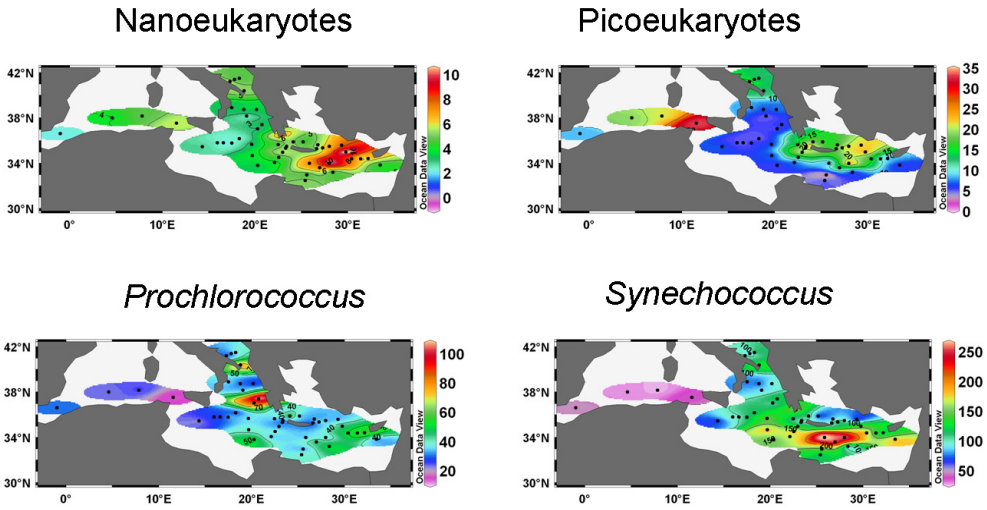

Fig. 5. Abundance distribution of ultraphytoplankton integrated between 0 to 200 m in the eastern Mediterranean, namely nanoeukaryotes, picoeukaryotes, *Prochlorococcus* and *Synechococcus*. Values are expressed with, as unit, 10^{10} cells m^{-2}. Dots denote the sampled stations. Note that different abundance scales were used.

BGD
6, 6839–6887, 2009

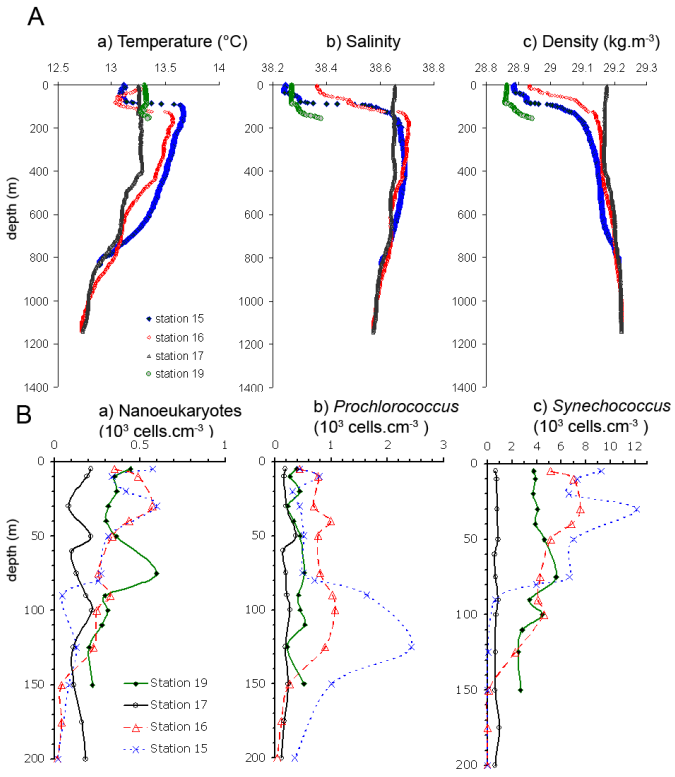

Fig. 6. Southern Adriatic features. A: Profiles of **(a)** temperature, **(b)** salinity, and **(c)** density excess for the stations located in the southern Adriatic and in the Strait of Otranto. B: Vertical distribution of **(a)** Nanoeukaryotes, **(b)** Prochlorococcus and **(c)** Synechococcus in the southern Adriatic and in the Strait of Otranto. Note that different scales of abundance are used for the sake of the presentation.

BGD
6, 6839–6887, 2009

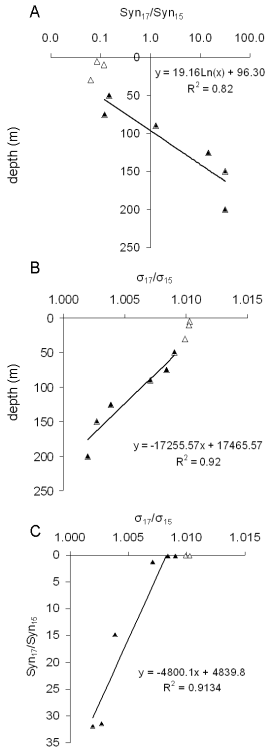

Fig. 7. Relationships between vertical distributions of *Synechococcus* abundance and density inside (station 17) and outside (station 15) the south Adriatic gyre. **(a)** Depth dependence of the abundance ratio Syn_{17}/Syn_{15}. **(b)** Depth dependence of the density ratio σ_{17}/σ_{15}. **(c)** Relationship between *Synechococcus* abundance ratio Syn_{17}/Syn_{15} and density ratio σ_{17}/σ_{15}. Data belonging to the upper 50 m (empty triangles) were excluded from the relationships (filled triangles).

BGD
6, 6839–6887, 2009

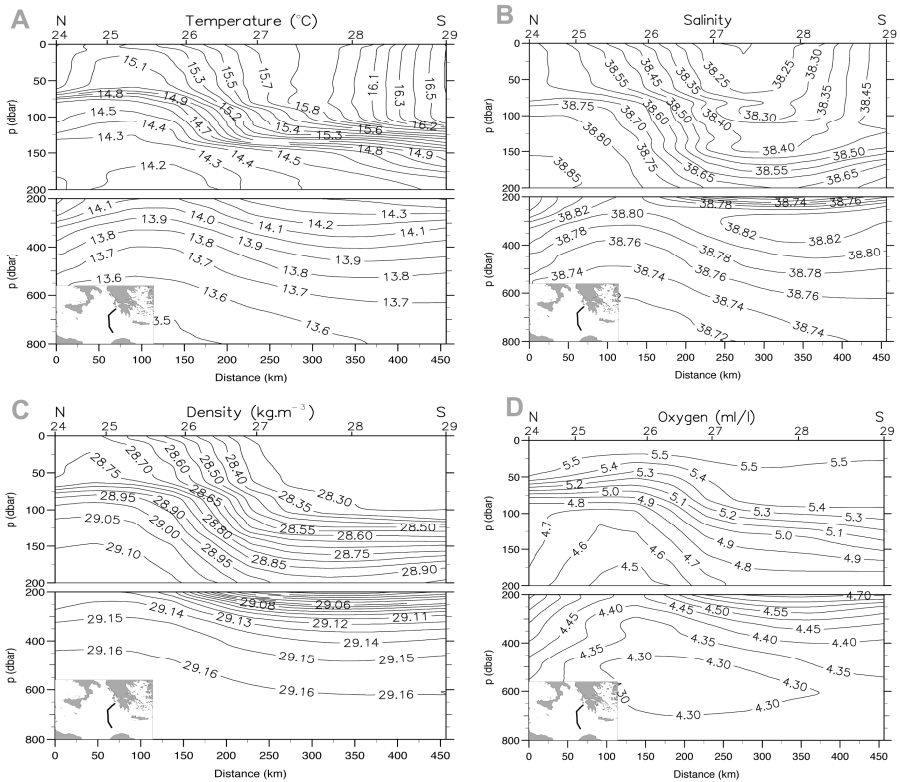

Fig. 8. Vertical distribution of **(a)** temperature, **(b)** salinity, **(c)** density and **(d)** dissolved oxygen along the north-south transect defined by stations 24 to 29. To note the presence of an eddy field establishing a thermohaline front located between stations 25 and 27.

BGD
6, 6839–6887, 2009

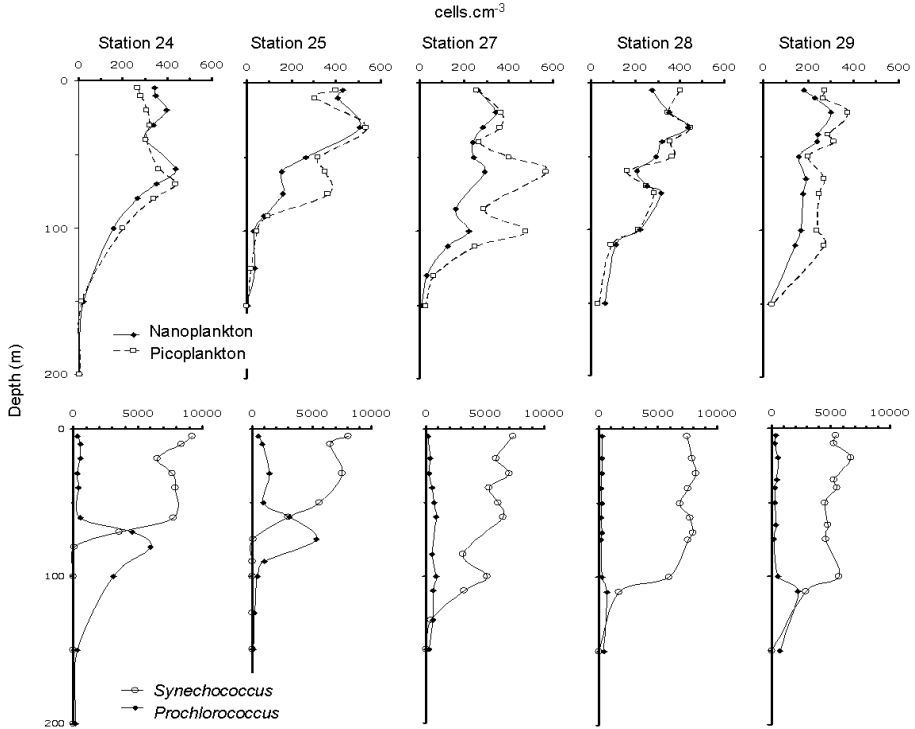

Fig. 9. Vertical profiles of ultraphytoplankton at stations 24 to 29 located along the transect crossing the thermohaline front at the eastern Ionian, as evidenced in Fig. 8.

BGD
6, 6839–6887, 2009

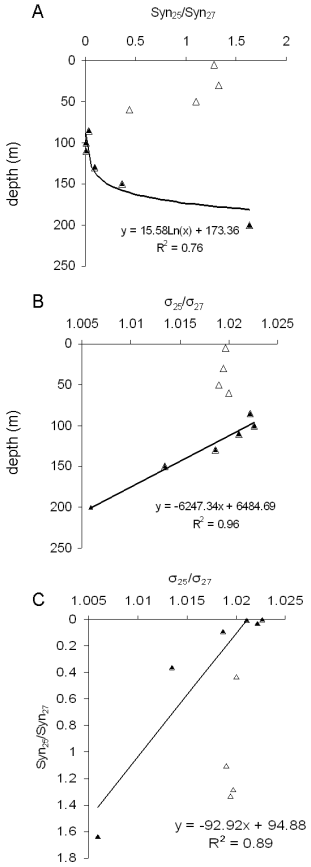

Fig. 10. Relationships between vertical distributions of *Synechococcus* abundance and density north (station 25) and south (station 27) of the thermohaline front. **(a)** Depth dependence of the abundance ratio Syn_{25}/Syn_{27}. **(b)** Depth dependence of the density ratio σ_{25}/σ_{27}. **(c)** Relationship between *Synechococcus* abundance ratio Syn_{25}/Syn_{27} and density ratio σ_{25}/σ_{27}.

BGD
6, 6839–6887, 2009

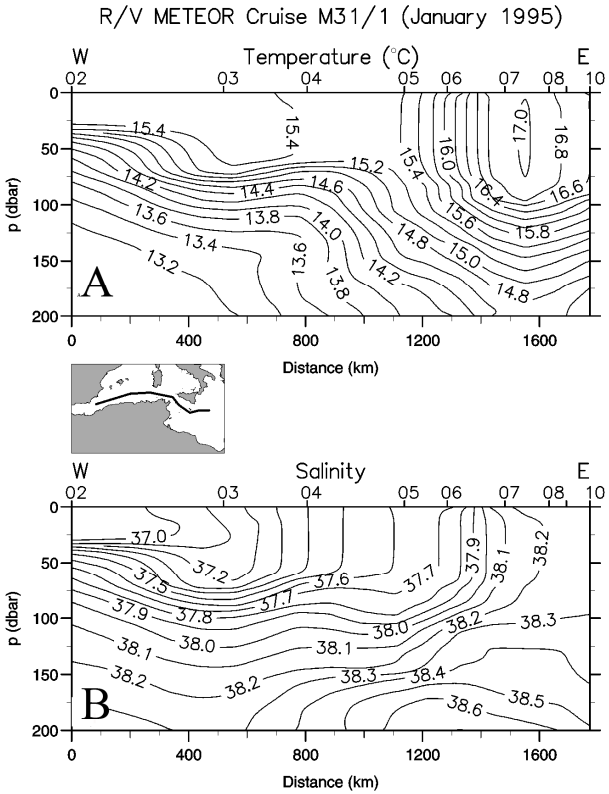

Fig. 11. Vertical distribution of **(a)** temperature and **(b)** salinity across the western Mediterranean Basin and the western part of the Ionian Sea illustrating the difference in temperature and salinity on both sides of the Sicily Strait.

BGD
6, 6839–6887, 2009

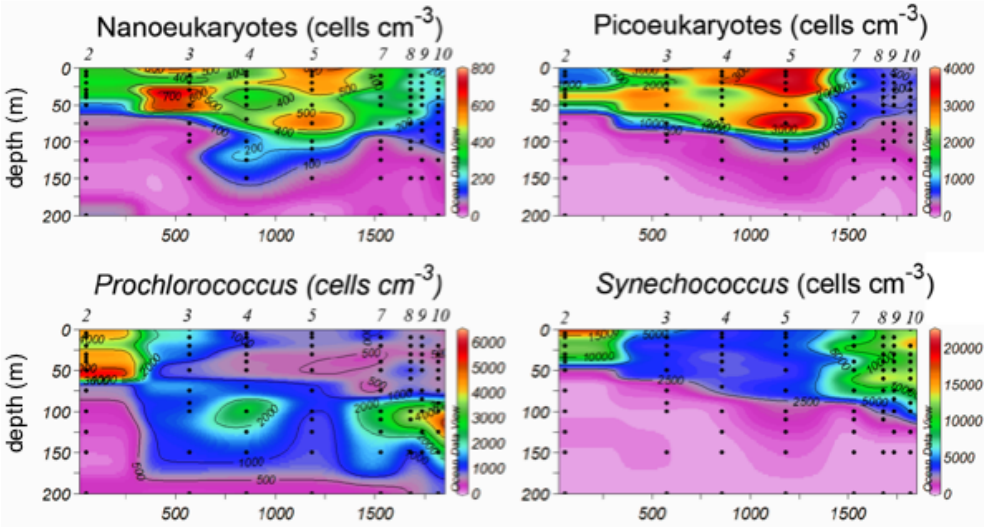

Fig. 12. Vertical distribution of ultraphytoplankton along the transect defined by stations 2 to 10, namely nanoeukaryotes, picoeukaryotes, *Prochlorococcus* and *Synechococcus*. Note that station 5 (Sicily Strait) delimits a clear transition for all distributions between the western and eastern Basins.

BGD
6, 6839–6887, 2009

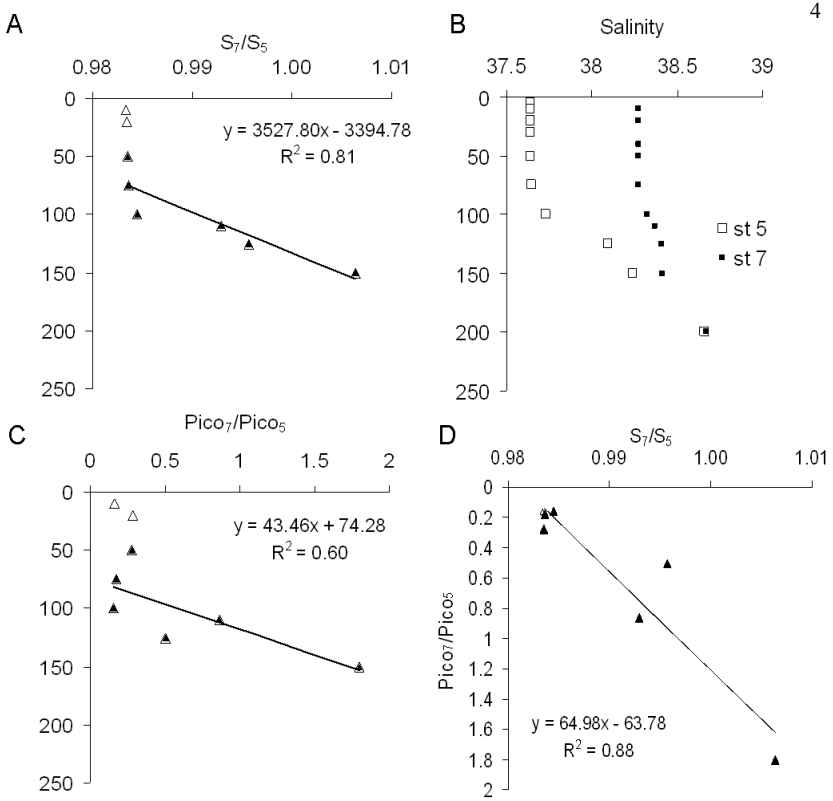

Fig. 13. Relationships between vertical distributions of picoeukaryote (Pico) abundance and salinity in the western (station 5) and eastern (station 7) Mediterranean. **(a)** Depth dependence of the salinity ratio S_7/S_5. **(b)** Vertical distribution of salinity. **(c)** Depth dependence of the abundance ratio $Pico_7/Pico_5$. **(d)** Relationship between picoeukaryote abundance ratio $Pico_7/Pico_5$ and salinity ratio S_7/S_5.

BGD
6, 6839–6887, 2009